ISSN 0253-9837
CN 21-1601/O6

催化学报 Chinese Journal of Catalysis

www.cjcatal.org

Volume 42 | Number 2 | February 2021

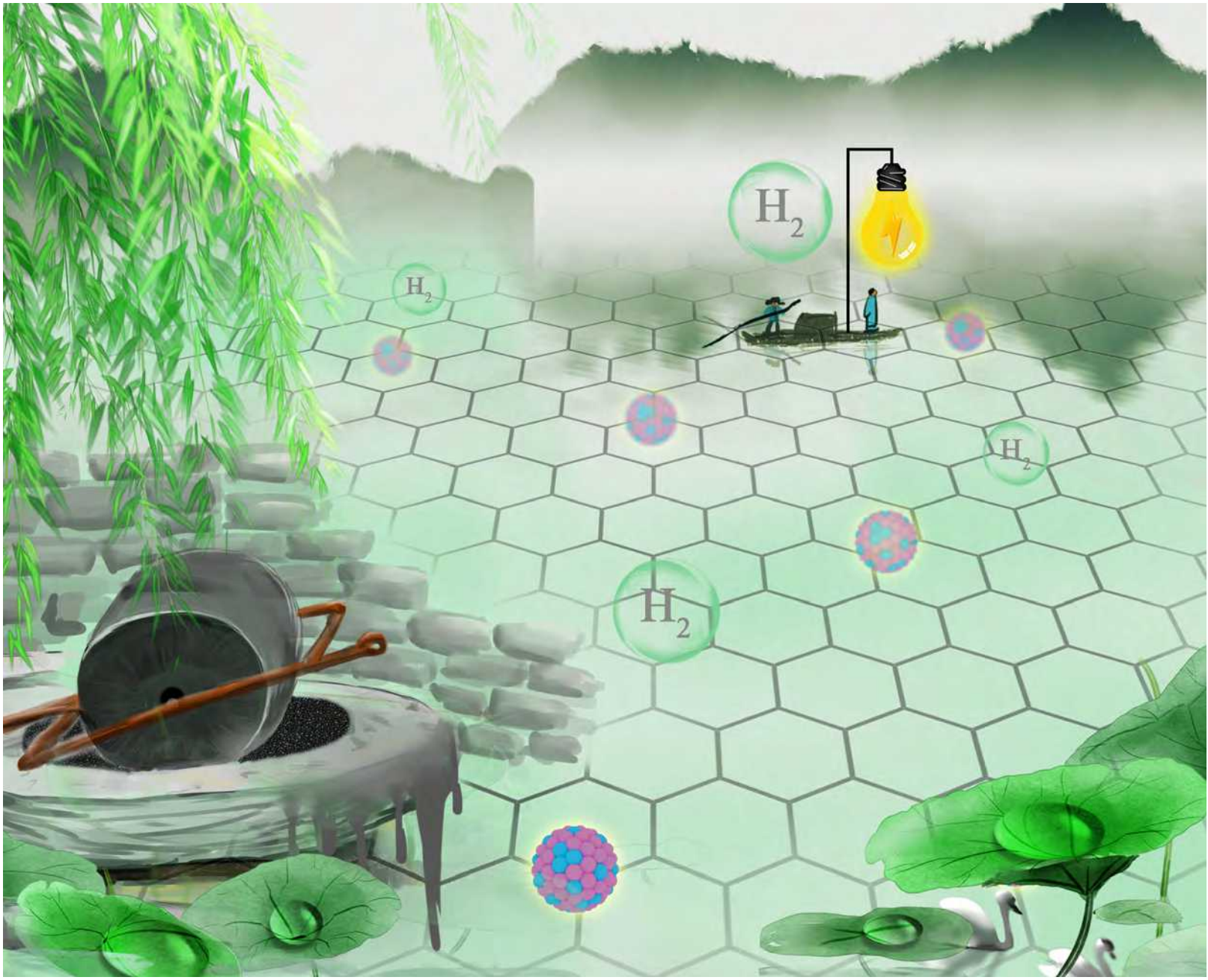

催化学报 CHINESE JOURNAL OF CATALYSIS February 2021 Vol. 42 No. 2 Pages 245-366

科学出版社

Science Press
CCS 中国化学会 CHINESE CHEMICAL SOCIETY

Editors-in-Chief Can Li Tao Zhang
Transaction of The Catalysis Society of China

2021
Vol. 42 No. 2

Chinese Journal of Catalysis

2021年
第42卷 第2期

In This Issue

Cover: Dr. Zhang and Prof. Fan in their article on pages 251–258 reported a facile grinding strategy to successfully produce a series of PdAg alloy nanoparticles with a small size and good distribution on the carbon matrix. Those samples as the electrocatalysts could exhibit excellent activities and stabilities for the alkaline hydrogen oxidation and evolution reactions.

封面: 张云和樊光银等发展了一种可持续化策略, 即于室温下在玛瑙研钵中直接研磨合成了一系列高分散在碳载体上的小尺寸 PdAg 合金纳米颗粒. 此法无需任何溶剂和有机试剂, 整个过程简单便捷、绿色环保, 同时确保了 PdAg 合金纳米颗粒表面清洁无污染. 将系列样品用于碱性电催化氢氧化和析氢反应时, 均展现出高的催化性能. 见本期第 251–258 页.

About the Journal

Chinese Journal of Catalysis is an international journal published monthly by Chinese Chemical Society, Dalian Institute of Chemical Physics, Chinese Academy of Sciences, and Elsevier. The journal publishes original, rigorous, and scholarly contributions in the fields of heterogeneous and homogeneous catalysis in English or in both English and Chinese. The scope of the journal includes:

- New trends in catalysis for applications in energy production, environmental protection, and production of new materials, petroleum chemicals, and fine chemicals;
- Scientific foundation for the preparation and activation of catalysts of commercial interest or their representative models;
- Spectroscopic methods for structural characterization, especially methods for in situ characterization;
- New theoretical methods of potential practical interest and impact in the science and applications of catalysis and catalytic reaction;
- Relationship between homogeneous and heterogeneous catalysis;
- Theoretical studies on the structure and reactivity of catalysts.
- The journal also accepts contributions dealing with photo-catalysis, bio-catalysis, and surface science and chemical kinetics issues related to catalysis.

Types of Contributions

- ***Reviews*** deal with topics of current interest in the areas covered by this journal. Reviews are surveys, with entire, systematic, and important information, of recent progress in important topics of catalysis. Rather than an assemblage of detailed information or a complete literature survey, a critically selected treatment of the material is desired. Unsolved problems and possible developments should also be discussed. Authors should have published articles in the field. Reviews should have more than 80 references.
- ***Communications*** rapidly report studies with significant innovation and major academic value. They are limited to four Journal pages. After publication, their full-text papers can also be submitted to this or other journals.
- ***Articles*** are original full-text reports on innovative, systematic and completed research on catalysis.
- ***Highlights*** describe and comment on very important new results in the original research of a third person with a view to highlight their significance. The results should be presented clearly and concisely without the comprehensive details required for an original article.
- ***Perspectives*** are short reviews of recent developments in an established or developing topical field. The authors should offer a critical assessment of the trend of the field, rather than a summary of literatures.
- ***Viewpoints*** describe the results of original research in general in some area, with a view to highlighting the progress, analyzing the major problems, and commenting the possible research target and direction in the future.

Impact Factor

2018 SCI Impact Factor: **4.914**
2018 SCI 5-Year Impact Factor: 3.618

Abstracting and Indexing

Abstract Journals (VINITI)
Cambridge Scientific Abstracts (CIG)
Catalysts & Catalysed Reactions (RSC)
Current Contents/Engineering, Computing and Technology (Clarivate Analytics ISI)
Chemical Abstract Service/SciFinder (CAS)
Chemistry Citation Index (Clarivate Analytics ISI)
Japan Information Center of Science and Technology
Journal Citation Reports/Science Edition (Clarivate Analytics ISI)
Science Citation Index Expanded (Clarivate Analytics ISI)
SCOPUS (Elsevier)
Web of Science (Clarivate Analytics ISI)

available at www.sciencedirect.com

ScienceDirect

journal homepage: www.elsevier.com/locate/chnjc

Chinese Journal of Catalysis

Graphical Contents

Communication

Chin. J. Catal., 2021, 42: 245–250 doi: 10.1016/S1872-2067(20)63659-2

Evolution of catalytic activity driven by structural fusion of icosahedral gold cluster cores

Dan Yang, Yan Zhu *
Nanjing University

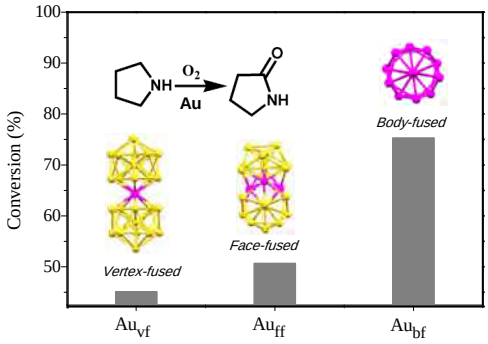

Atomically precise gold cluster catalysts have emerged as a new frontier in catalysis science and exhibited unexpected catalytic properties. Here, we demonstrate that the structural fusion of icosahedral Au_{13} cores to form vertex-fused (vf), face-fused (ff), and body-fused (bf) structures can control the catalytic activity of the clusters.

Articles

Chin. J. Catal., 2021, 42: 251–258 doi: 10.1016/S1872-2067(20)63650-6

Sustainable solid-state synthesis of uniformly distributed PdAg alloy nanoparticles for electrocatalytic hydrogen oxidation and evolution

Caili Xu, Qian Chen, Rong Ding, Shengtian Huang, Yun Zhang *, Guangyin Fan *
Sichuan Normal University;
Sichuan University of Science and Engineering

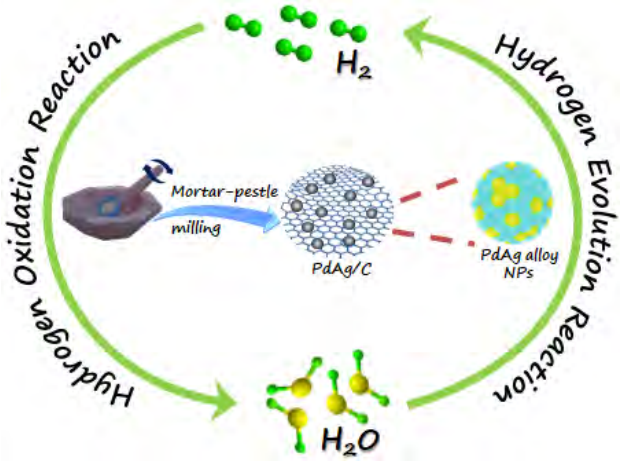

A facile grinding strategy is developed to produce a series of PdAg alloy NPs that are highly dispersed on various carbon supports. The resulting electrocatalysts exhibit excellent activities and stabilities in both the HOR and HER.

Chin. J. Catal., 2021, 42: 259–270 doi: 10.1016/S1872-2067(20)63629-4

Photocatalytic Cr(VI) elimination over BUC-21/N-$K_2Ti_4O_9$ composites: Big differences in performance resulting from small differences in composition

Xun Wang, Yu-Xuan Li, Xiao-Hong Yi, Chen Zhao, Peng Wang, Jiguang Deng *, Chong-Chen Wang *
Beijing University of Civil Engineering and Architecture;
Beijing University of Technology

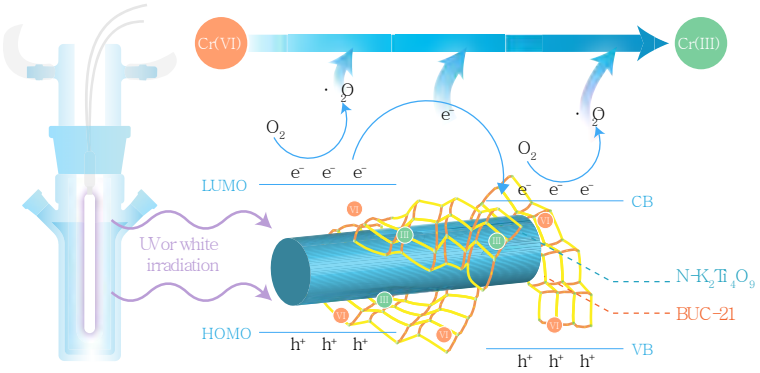

BUC-21/N-$K_2Ti_4O_9$ composites show high photocatalytic activity under UV and white light, which can be used to reduce Cr(VI) to Cr(III) effectively.

Chin. J. Catal., 2021, 42: 271–278 doi: 10.1016/S1872-2067(20)63639-7

Direct growth of holey Fe_3O_4-coupled $Ni(OH)_2$ sheets on nickel foam for the oxygen evolution reaction

Yu Ding, Bo-Qiang Miao, Yue Zhao, Fu-Min Li, Yu-Cheng Jiang *, Shu-Ni Li *, Yu Chen
Shaanxi Normal University

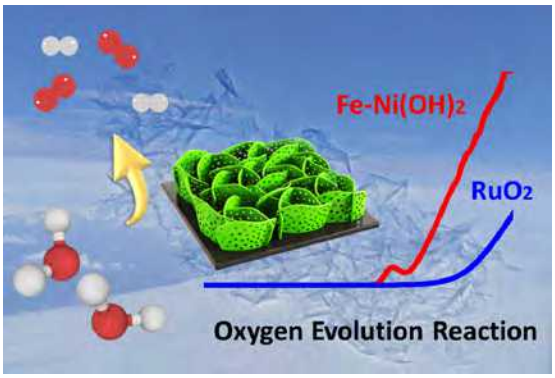

Herein, ultrathin holey Fe_3O_4-coupled $Ni(OH)_2$ sheets ($Ni(OH)_2$-Fe H-STs) were easily synthesized, which showed outstanding activity for the OER due to special structural features and synergistic effect between the Fe and Ni atom.

Chin. J. Catal., 2021, 42: 279–287 doi: 10.1016/S1872-2067(20)63625-7

Morphology evolution of acetic acid-modulated MIL-53(Fe) for efficient selective oxidation of H_2S

Xiaoxiao Zheng, Sihui Qi, Yanning Cao, Lijuan Shen *, Chaktong Au, Lilong Jiang *
Fuzhou University

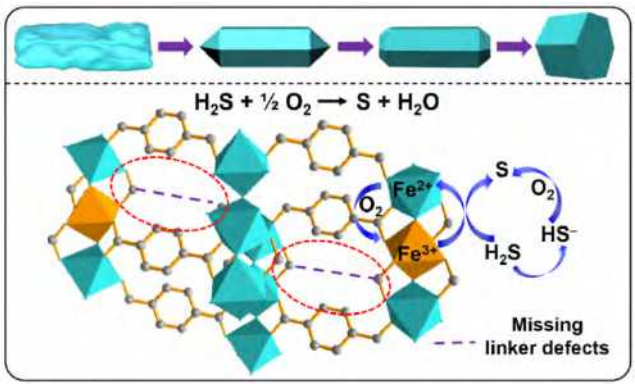

Using acetic acid coordination modulation, a series of MIL-53(Fe) with morphology evoluting from irregular bulky particles to highly uniform short hexagonal prisms were synthesized and applied for H_2S selective oxidation.

Chin. J. Catal., 2021, 42: 288–296 doi: 10.1016/S1872-2067(20)63643-9

Orbital symmetry matching: Achieving superior nitrogen reduction reaction over single-atom catalysts anchored on Mxene substrates

Jiale Qu, Jiewen Xiao, Hetian Chen, Xiaopeng Liu, Tianshuai Wang, Qianfan Zhang *
Beihang University

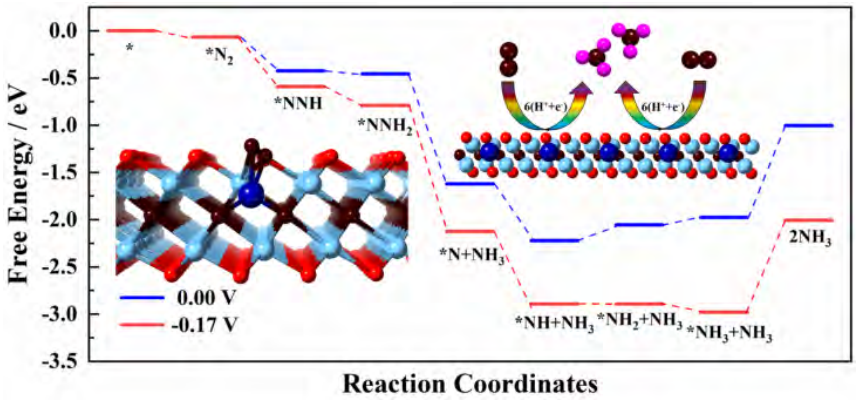

Single atom doped on MXene, which can synergize with the adjacent titanium atom on the matrix. With this synergy, the nitrogen reduction reaction can be proceeded at a low limiting potential.

Chin. J. Catal., 2021, 42: 297–309 doi: 10.1016/S1872-2067(20)63658-0

Honeycomb-structured solid acid catalysts fabricated via the swelling-induced self-assembly of acidic poly(ionic liquid)s for highly efficient hydrolysis reactions

Bihua Chen, Tong Ding, Xi Deng, Xin Wang, Dawei Zhang, Sanguan Ma, Yongya Zhang, Bing Ni, Guohua Gao *
East China Normal University, China; University of Cambridge, U.K.

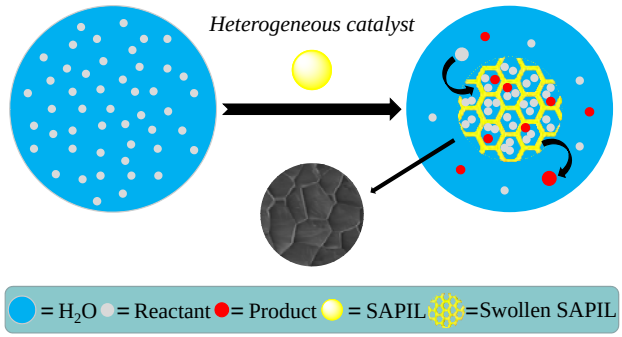

The catalytic activity of SAPILs with micron-sized 3D honeycomb structure in water and high enrichment ability for the reactants of hydrolysis and hydration reactions was much higher than that of homogeneous acid catalysts.

Chin. J. Catal., 2021, 42: 310–319 doi: 10.1016/S1872-2067(20)63644-0

Selective photocatalytic reduction of CO_2 to CO mediated by a [FeFe]-hydrogenase model with a 1,2-phenylene S-to-S bridge

Minglun Cheng, Xiongfei Zhang, Yong Zhu, Mei Wang *
Dalian University of Technology

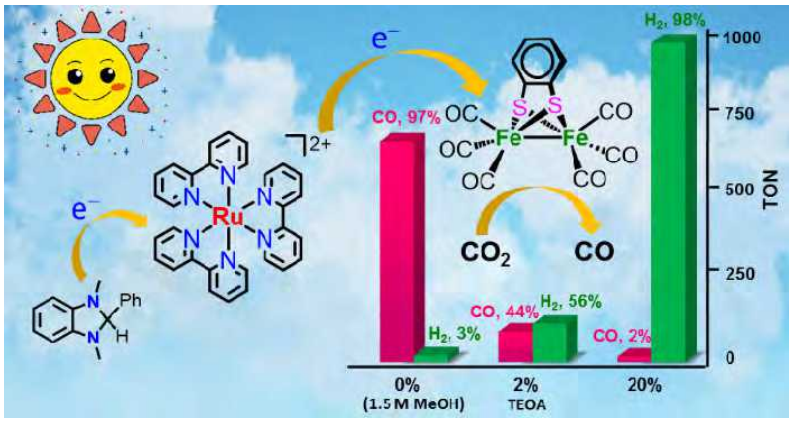

An [FeFe]-hydrogenase model was demonstrated to be highly active for the photochemical reduction of CO_2 with a TOF of 7.12 min^{-1} and CO selectivity of 97%. The CO/H_2 ratio can be adjusted by the addition of TEOA.

Chin. J. Catal., 2021, 42: 320–333 doi: 10.1016/S1872-2067(20)63636-1

Small-sized cuprous oxide species on silica boost acrolein formation via selective oxidation of propylene

Ling-Ling Guo, Jing Yu, Wei-Wei Wang, Jia-Xu Liu *, Hong-Chen Guo, Chao Ma *, Chun-Jiang Jia *, Jun-Xiang Chen, Rui Si *
Shanghai Institute of Applied Physics, Chinese Academy of Sciences; Shanghai Synchrotron Radiation Facility, Zhangjiang Laboratory; Shanghai Institute of Measurement and Testing Technology; Shandong University; Dalian University of Technology; Hunan University; TILON Group Technology Limited; University of Chinese Academy of Science

Small-sized copper oxide clusters have been fabricated on silica for the efficient formation of acrolein via the selective oxidation of propylene. The reaction mechanism was explored using *in situ* X-ray diffraction and *in situ* dual beam Fourier transform infrared spectroscopy.

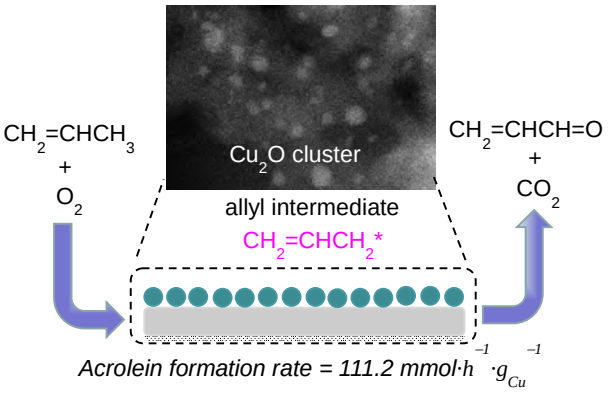

Chin. J. Catal., 2021, 42: 334–346 doi: 10.1016/S1872-2067(20)63617-8

Acetylene hydrochlorination over supported ionic liquid phase (SILP) gold-based catalyst: Stabilization of cationic Au species via chemical activation of hydrogen chloride and corresponding mechanisms

Jia Zhao *, Saisai Wang, Bolin Wang, Yuxue Yue, Chunxiao Jin, Jinyue Lu, Zheng Fang, Xiangxue Pang, Feng Feng, Lingling Guo, Zhiyan Pan, Xiaonian Li *
Zhejiang University of Technology

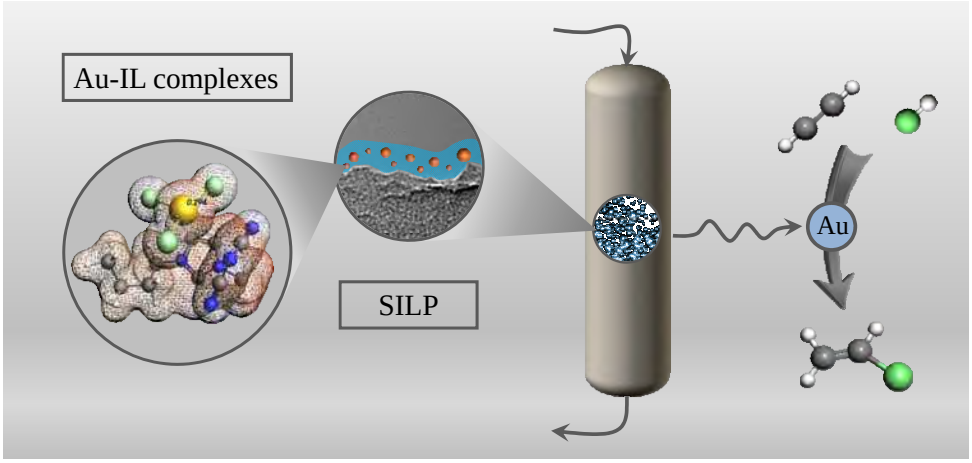

Cationic Au species coordinate with [Bmim][N(CN)$_2$] to form strong Au-IL complexes, which greatly increase the thermal and reaction stability of Au-based catalysts.

Chin. J. Catal., 2021, 42: 347–355 doi: 10.1016/S1872-2067(20)63668-3

Complete removal of phenolic contaminants from bismuth-modified TiO_2 single-crystal photocatalysts

Wenjie Tang, Juanrong Chen, Zhengliang Yin, Weichen Sheng *, Fengjian Lin, Hui Xu, Shunsheng Cao *
Jiangsu University

The Bi-SCTiO$_2$ photocatalyst exhibits complete degradation of phenolic contaminants under simulated sunlight due to the synergistic effect of the small band overlap and the low charge carrier density (Bi) as well as high conductivity (single crystal).

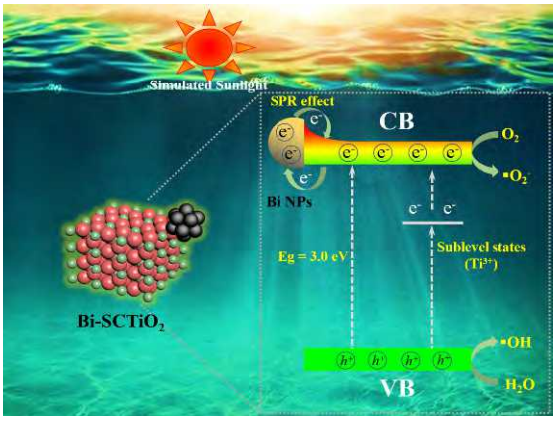

Chin. J. Catal., 2021, 42: 356–366 doi: 10.1016/S1872-2067(20)63665-8

Solvothermal synthesis of Co-substituted phosphomolybdate acid encapsulated in the UiO-66 framework for catalytic application in olefin epoxidation

Dianwen Hu, Xiaojing Song, Shujie Wu, Xiaotong Yang, Hao Zhang, Xinyu Chang, Mingjun Jia *
Jilin University

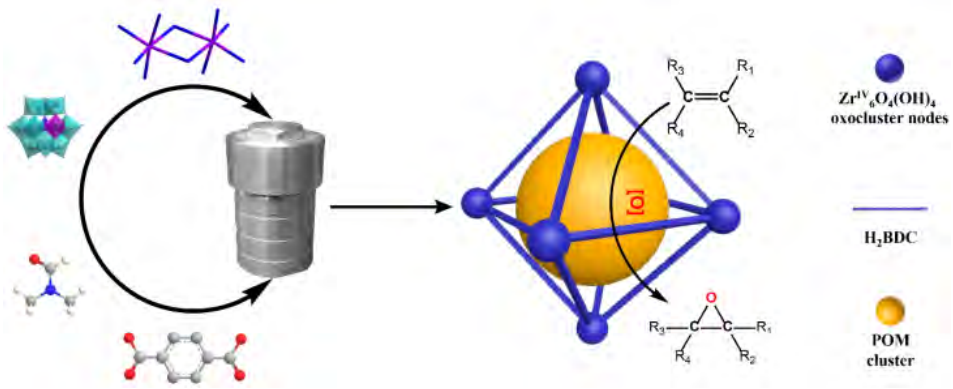

Hybrid composites based on Co-substituted phosphomolybdic acid ($PMo_{11}Co$) and UiO-66 were synthesized by the direct solvothermal method. $PMo_{11}Co$@UiO-66 showed high catalytic activity and stability for the epoxidation of a variety of olefins with *t*-BuOOH as the oxidant.

中国科学院科学出版基金资助出版

催化学报 Chinese Journal of Catalysis

月刊 SCI收录 2021年2月 第42卷 第2期

目 次

快 讯

论 文

英文全文电子版(国际版)由Elsevier出版社在ScienceDirect上出版
http://www.sciencedirect.com/science/journal/18722067
http://www.elsevier.com/locate/chnjc
www.cjcatal.org
在线投审稿网址
https://mc03.manuscriptcentral.com/cjcatal

available at www.sciencedirect.com

ScienceDirect

journal homepage: www.elsevier.com/locate/chnjc

Article

Photocatalytic Cr(VI) elimination over BUC-21/N-$K_2Ti_4O_9$ composites: Big differences in performance resulting from small differences in composition

Xun Wang [a], Yu-Xuan Li [a], Xiao-Hong Yi [a], Chen Zhao [a], Peng Wang [a], Jiguang Deng [b,*], Chong-Chen Wang [a,#]

[a] *Beijing Key Laboratory of Functional Materials for Building Structure and Environment Remediation, School of Environment and Energy Engineering, Beijing University of Civil Engineering and Architecture, Beijing 100044, China*

[b] *Department of Chemistry and Chemical Engineering, College of Environmental and Energy Engineering, Beijing University of Technology, Beijing 100022, China*

ARTICLE INFO

Article history:
Received 23 March 2020
Accepted 5 May 2020
Published 5 February 2021

Keywords:
BUC-21
N-$K_2Ti_4O_9$
Photocatalysis
Hexavalent chromium
UV and white light

ABSTRACT

A series of BUC-21/N-$K_2Ti_4O_9$ composites (B1N*X*) were facilely fabricated from BUC-21 and N-$K_2Ti_4O_9$ via ball-milling, and they were fully characterized using various techniques. The photocatalytic reduction of Cr(VI) over the B1N*X* composites was investigated systematically under various conditions, including different light sources, pH values, hole scavengers, and inorganic ions, in both real lake water and tap water. The BUC-21/N-$K_2Ti_4O_9$ composites demonstrated remarkable photocatalytic Cr(VI) reduction performance, good reusability, and stability under both UV and white light irradiation. The introduction of N-$K_2Ti_4O_9$ into BUC-21 not only broadened its light absorption region to white light, but also strongly inhibited the recombination of the photo-generated electrons and holes. Mechanisms of photocatalytic Cr(VI) reduction under both UV light and white light were proposed and verified by electrochemical measurements, active species capture experiments, and ESR measurements.

© 2021, Dalian Institute of Chemical Physics, Chinese Academy of Sciences. Published by Elsevier B.V. All rights reserved.

1. Introduction

Due to increasing industrialization, hexavalent chromium (Cr(VI)), which is produced mainly from electroplating, photography, mining, and other processes [1–3], has become an important research topic in wastewater treatment [4–6]. The presence of Cr(VI) in water negatively affects the environment and increases the risk of some cancers [7–9]. Therefore, the removal of Cr(VI) from water is necessary. Among the various treatment methods available, including adsorption, electro-reduction, chemical reduction, and others, photocatalysis is typically used to reduce highly toxic Cr(VI) to low-toxicity Cr(III) because of its simple working conditions and environmental sustainability [10–12].

Metal-organic frameworks (known as MOFs) and coordination polymers (CPs) are periodic porous materials with ultra-high porosity and are constructed from metal ions or clusters and organic linkers through coordinative bonding interac-

* Corresponding author. Tel/Fax: +86-10-61209186; E-mail: jgdeng@bjut.edu.cn
# Corresponding author. E-mail: wangchongchen@bucea.edu.cn, chongchenwang@126.com

This work was supported by the National Natural Science Foundation of China (51878023), Beijing Natural Science Foundation (8202016), Great Wall Scholars Training Program Project of Beijing Municipality Universities (CIT&TCD20180323), Beijing Talent Project (2019A22), and BUCEA Post Graduate Innovation Project (PG2019038).
DOI: 10.1016/S1872-2067(20)63629-4 | http://www.sciencedirect.com/science/journal/18722067 | Chin. J. Catal., Vol. 42, No. 2, February 2021

tions and self-assembly [13–15]. Due to their advantages of various synthesis methods and adjustable active sites, MOFs and CPs are considered star materials and are widely studied in the field of gas adsorption/separation [16–18], sensing [19–21], catalysis [22–24], and absorptive pollutant removal applications [25]. In recent years, MOFs and CPs have been adopted as efficient photocatalysts to accomplish photocatalytic Cr(VI) reduction [26,27], photocatalytic CO_2 reduction [28,29], photocatalytic decomposition of organic pollutants [30,31], and photocatalytic H_2 production via water splitting [32,33]. However, disadvantages such as low conductivity, fast recombination of electrons and holes, and limited response under UV light have inhibited their photocatalytic activities. To overcome these problems, several strategies involving the fabrication of composites of MOFs or CPs with semiconductors (such as g-C_3N_4 [34,35], Ag_2CO_3 [36], TiO_2 [37], and $Bi_{24}O_{31}Br_{10}$ [38]), electroactive polymers (such as PANI [39]), conductors (like RGO [40]), and noble metal nanoparticles (such as Ag [41] and Pd [42]) have been introduced. BUC-21 is a stable 2D coordination polymer produced by our research group using *cis*-1,3-dibenzyl-2-oxo-4,5-imidazolidinedicarboxylic acid (H_2L) and 4,4′-bipyridine (bpy) as organic linkers and Zn^{2+} as the metal ion. BUC-21 exhibited superior photocatalytic performance toward Cr(VI) reduction and organic pollutant decomposition under UV light [43]. Furthermore, g-C_3N_4 [44] and $Bi_{24}O_{31}Br_{10}$ [38] were introduced to broaden the light absorption range of BUC-21 from the UV region to the visible region and enhance its photocatalytic activity. $K_2Ti_4O_9$ is a two-dimensional layered material composed of octahedral TiO_2 units bridged by oxygen atoms [45]. Because of its low cost, non-toxicity, and distinctive photoelectric properties, it has been recognized a potential photocatalyst. However, due to its wide band gap (3.2–3.4 eV), it is only responsive to UV light [46]. Doping nitrogen into $K_2Ti_4O_9$ is a convenient and effective way to adjust its band gap, as has been confirmed by previous works [47,48]. In this study, N-$K_2Ti_4O_9$ was successfully synthesized by a calcination method, and BUC-21/N-$K_2Ti_4O_9$ composites were prepared by ball milling. The structure, morphology, and photoelectric performance of the BUC-21/ N-$K_2Ti_4O_9$ composites were characterized and measured, and their photocatalytic activities were assessed under ultraviolet (UV) and white light irradiation. The results indicated that the introduction of N-$K_2Ti_4O_9$ increased the Cr(VI) reduction efficiency of the composites under both UV and white light; this improvement was attributed to the accelerated separation of the photo-generated electrons and holes due to the rapid electron transfer between N-$K_2Ti_4O_9$ and BUC-21. Additionally, the composites exhibited good stability and recyclability after five runs of the photocatalytic reaction. Finally, mechanisms for the catalysis were proposed and confirmed.

2. Experimental

2.1. Materials and instruments

The chemicals and the characterization instruments used in this work are described in the electronic supplementary information (ESI).

2.2. Preparation of photocatalysts

2.2.1. Synthesis of BUC-21, $K_2Ti_4O_9$, and N-$K_2Ti_4O_9$

BUC-21, $K_2Ti_4O_9$, and N-$K_2Ti_4O_9$ were prepared according to previous reports [43,49,50]. Detailed preparation procedures are given in the ESI.

2.2.2. Preparation of BUC-21/N-$K_2Ti_4O_9$

The BUC-21/N-$K_2Ti_4O_9$ composites were fabricated by ball-milling treatment of mixtures of BUC-21 and N-$K_2Ti_4O_9$ at 30 Hz for 20 min. The ratios of BUC-21 and N-$K_2Ti_4O_9$ in the various composites are listed in Table 1.

2.3. Photocatalytic activity of ***B1NX***

The photocatalytic performances of the B1N*X* composites were assessed via the photoreduction of Cr(VI) to Cr(III). A 200 mL of an aqueous solution of $K_2Cr_2O_7$ (10 mg L^{-1}) containing 0.175 g L^{-1} photocatalyst was irradiated with either UV light (Hg lamp with an optical power of 153.5 mW, Beijing Aulight Co., Ltd) and white light (Xe lamp with an optical power of 598 mW, Beijing Aulight Co., Ltd). The spectra of the UV lamp and white lamp are shown in Fig. S1. Before illumination, the suspension was continually stirred in the dark to achieve adsorption-desorption equilibrium. During illumination, 1.5 mL of the solution was extracted every 10 min using a 0.22 μm filter for subsequent detection. The Cr(VI) concentration was measured using the diphenylcarbazide (DPC) method with an AutoAnalyzer 3 instrument. The pH values of the suspension were adjusted from 2.0 to 8.0 using 0.1 M H_2SO_4 and 0.1 M NaOH solutions.

The apparent quantum efficiencies (AQE) of B1N0.5 and B1N3 toward Cr(VI) reduction upon irradiation with various frequencies of monochromatic light were calculated according to Eqs. 1 and 2, as described in previous studies [23,51,52]. The average irradiance values were measured using a cell-np2000-2 optical power meter.

$$\text{AQE (Cr)} = \frac{3\times[\text{number of reduced Cr (VI)}]}{\text{number of incident photons}} \quad (1)$$

$$N_P^i = \frac{\bar{\lambda} t A_R \bar{E}}{hc}, \quad (2)$$

where $N_p{}^i$ is the number of incident photons; $\overline{\lambda}$ is the irradiation wavelength (m); t is the irradiation time (s); A_R is the light-receiving area of the reactor (m^2); $\overline{E}$ is the average irradiance ($W\cdot m^{-2}$); h is the Planck constant, and c is the speed of

Table 1
Ratios of BUC-21 and N-$K_2Ti_4O_9$ used to prepare the BUC-21/N-$K_2Ti_4O_9$ composites.

No.	BUC-21/mg	N-$K_2Ti_4O_9$/mg	Code name
1	166.7	33.3	B1N0.2
2	133.3	66.6	B1N0.5
3	100	100	B1N1
4	66.7	133.3	B1N2
5	50	150	B1N3
6	40	160	B1N4

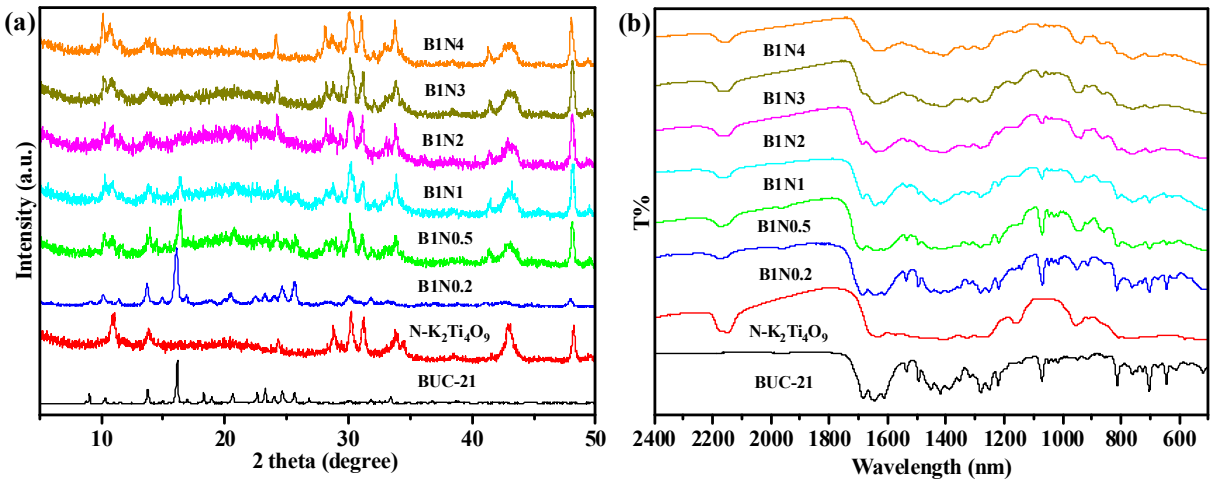

Fig. 1. (a) PXRD patterns and (b) FTIR spectra of BUC-21, N-$K_2Ti_4O_9$, and the series of B1N*X* composites.

light in a vacuum (m/s).

2.4. Electrochemical test

The electrochemical tests of B1N0.5 and B1N3 were carried out with reference to previous works [38,53], as described in the ESI.

3. Results and discussion

3.1. Characterizations

The PXRD patterns of BUC-21, N-$K_2Ti_4O_9$ and the series of BUC-21/N-$K_2Ti_4O_9$ (B1N*X*) composites are depicted in Fig. 1a. All composites showed peaks at 10.2°, 14.8°, 15.9°, and 24.5° originating from BUC-21 [43,44]. Additionally, the PXRD patterns of the synthesized N-$K_2Ti_4O_9$ matched well with those previously reported [54], in which the characteristic diffraction peaks at 10.9°, 13.7°, 24.3°, 28.7°, 30.3°, 31.2°, 33.6°, 43.1°, and 48.1° were attributed to the (2 0 0), (2 0 1), (1 1 0), (3 1 0), (3 1 1), (0 0 4), (– 3 1 3), (2 0 5), and (0 2 0) planes of N-$K_2Ti_4O_9$ [55]. To prove the structural stability of the composites, both BUC-21 and N-$K_2Ti_4O_9$ were characterized before and after ball milling by PXRD. The ball milling treatments did not bring about any noticeable changes to the crystal phase of BUC-21 (Fig. S2a). However, ball milling induced the exposure of additional crystal facets such as (–6 0 3) for N-$K_2Ti_4O_9$ (Fig. S2b), which were observed in the B1N*X* composites and were similar to a previous report [56]. The FTIR spectra also demonstrated the successful fabrication of the B1N*X* composites. As shown in Fig. 1b, the characteristic peaks of both BUC-21 and N-$K_2Ti_4O_9$ were observed in the spectra of the B1N*X* composites.

The particle sizes of the pristine BUC-21 ranged from 300 to 900 nm (Figs. 2a and S3a), and the pure N-$K_2Ti_4O_9$ exhibited a rod-like structure with a length of a few micrometers [46,57] (Figs. 2b and S3b). After ball-milling treatment, the BUC-21 particles were randomly distributed over the rod-like N-$K_2Ti_4O_9$, which can be observed by TEM (Figs. 2c and 2d) rather than SEM (Figs. S3c and S3d). TEM-EDS analysis was performed on selected regions of certain composites. The results showed that the B1N0.5 and B1N3 composite photocatalysts contained the elements Zn, N, K, and Ti; the presence of N, K, and Ti was attributed to N-$K_2Ti_4O_9$, and the Zn was introduced by BUC-21. The interaction between BUC-21 and N-$K_2Ti_4O_9$ was further affirmed by HRTEM observation (Fig. 4), in which the *d* spacings of 3.71, 2.95, and 3.18 Å corresponded to the (1 1 0), (3 1 1), and (3 1 0) planes of N-$K_2Ti_4O_9$.

As depicted in Fig. 5, obvious signals of the elements Zn, Ti, O, and N were observed in the XPS spectra of B1N0.5. The two obvious N 1*s* and Zn 2*p* peaks in the XPS survey spectrum in Fig. 5a were attributed to N-$K_2Ti_4O_9$ and BUC-21, respectively. The peaks at 1045.3 and 1022.3 eV (Fig. 5b) were ascribed to Zn $2p_{1/2}$ and Zn $2p_{3/2}$ of BUC-21 in B1N0.5, respectively [44]. The peaks at 464.0 and 458.2 eV (Fig. 5c) were assigned to Ti $2p_{1/2}$ and Ti $2p_{3/2}$ [58]. Three O 1*s* peaks with different binding energies (Fig. 5d) were observed, which were attributed to

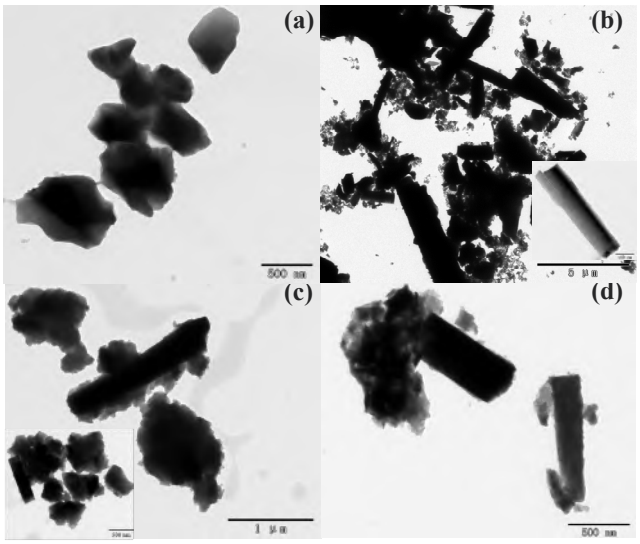

Fig. 2. TEM images of (a) pristine BUC-21, (b) pristine N-$K_2Ti_4O_9$, (c) B1N0.5, and (d) B1N3.

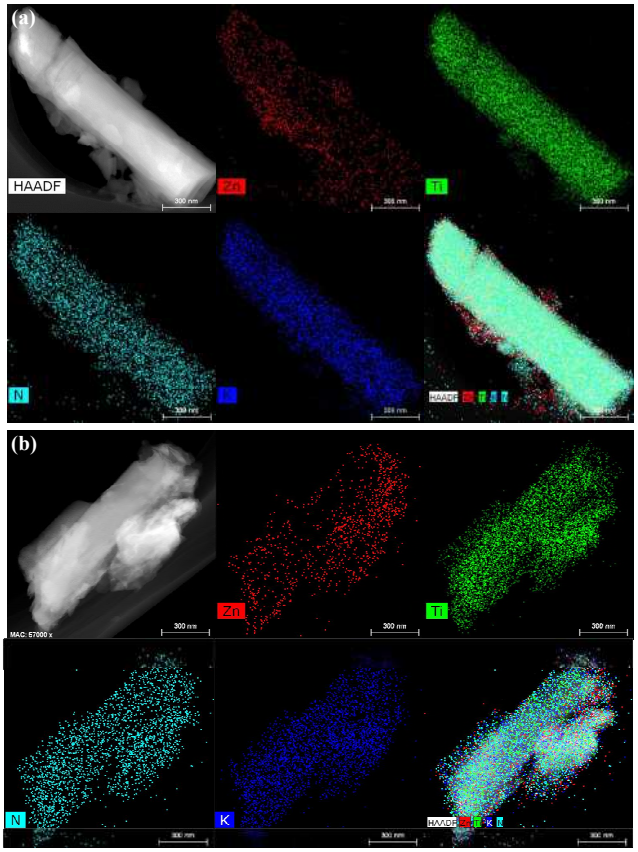

Fig. 3. EDS elemental mappings of (a) B1N0.5 and (b) B1N3.

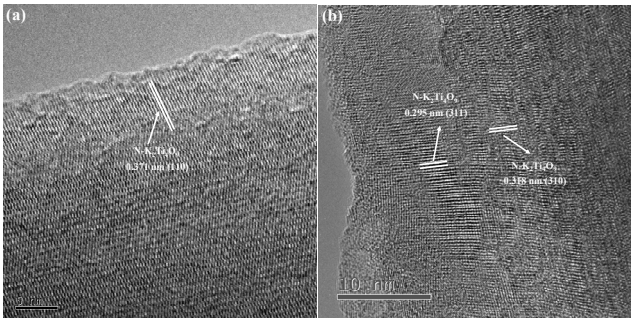

Fig. 4. HRTEM images of (a) **B1N0.5** and (b) **B1N3**.

O–H (532.0 eV), O–Zn (531.5 eV), and lattice oxygen (529.6 eV). Notably, the lattice oxygen peak (529.6 eV) was indicative of the existence of a Ti-O-Ti structure in N-$K_2Ti_4O_9$ [44,45]. The N 1*s* spectrum for B1N0.5 is presented in Fig. 5e; the 399.4 and 400.0 eV peaks revealed the presence of O-Ti-N and Ti-N-O or Ti-O-N, respectively [59,60]. Identical chemical composition and chemical states were observed in the XPS characterization of B1N3 (Fig. 6). In B1N3, the redistribution of additional electrons between BUC-21 and N-$K_2Ti_4O_9$ led to decreased binding energies for the lattice oxygen and O-Ti-N [44].

The UV-vis DRS spectra of the BUC-21, N-$K_2Ti_4O_9$, and B1N*X* composites are shown in Fig. 7a; the light absorption behavior of the B1N*X* composites approached that of N-$K_2Ti_4O_9$. The band-gap energy (E_g) of BUC-21, N-$K_2Ti_4O_9$, and the B1N*X* composites can be estimated according to the expression $\alpha h\upsilon = A(h\upsilon - E_g)^{n/2}$, as described in previous publications [61]. The results showed that the E_g values of the B1N*X* composites ranged from 2.91 to 2.99 eV. Based on the diffuse reflectance spectra, the band-edge wavelengths of the B1N*X* composites were at the junction of the ultraviolet absorption and visible absorption ranges, implying that the B1N*X* composites could be irradiated using both UV light and visible light.

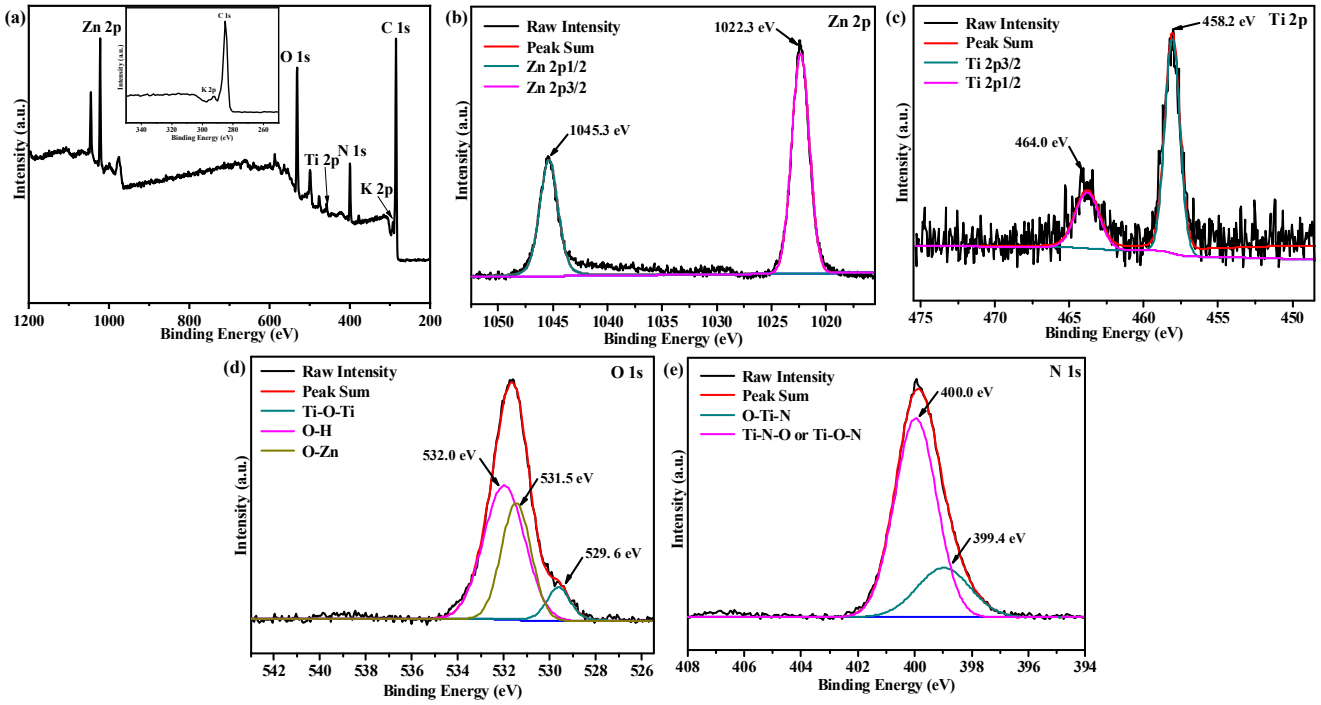

Fig. 5. (a) XPS survey spectrum, (b) Zn 2*p* spectrum, (c) Ti 2*p* spectrum, (d) O 1*s* spectrum, and (e) N 1*s* spectrum of B1N0.5.

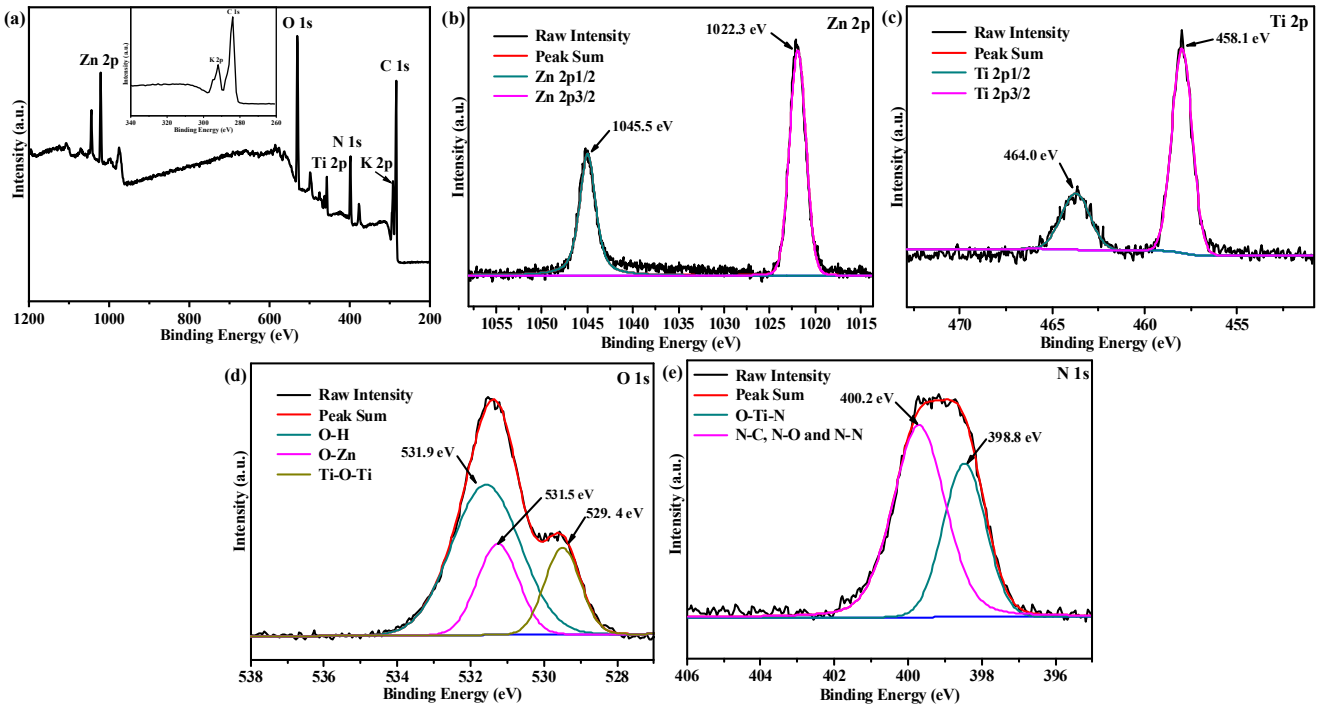

Fig. 6. (a) XPS survey spectrum, (b) Zn 2*p* spectrum, (c) Ti 2*p* spectrum, (d) O 1*s* spectrum, and (e) N 1*s* spectrum of B1N3.

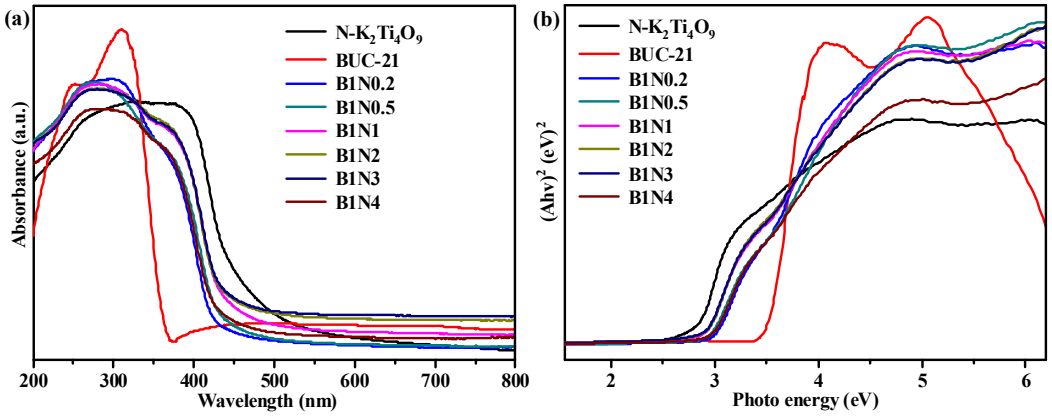

Fig. 7. (a) UV-vis DRS spectra and (b) E_g plots of BUC-21, N-$K_2Ti_4O_9$, and the series of B1NX composites.

3.2. *Photocatalytic performance of B1NX*

The adsorption of Cr(VI) by the composites under dark conditions was tested before carrying out photocatalytic reduction experiments. As shown in Figs. 8a and 8d, the adsorption of Cr(VI) on the BUC-21, N-$K_2Ti_4O_9$, and series of B1N*X* composites was so weak as to be negligible. Under UV light irradiation, the optimal composites B1N0.5 and B1N1 accomplished 100% Cr(VI) reduction within 40 min, which surpassed that of bare BUC-21 (94% within 40 min). The kinetics of the Cr(VI) reduction rate followed the order B1N0.5 > B1N1 > BUC-21. Under white light, the pristine BUC-21 and N-$K_2Ti_4O_9$ reduced less than 10% of the Cr(VI) after 130 min. The B1N*X* composites demonstrated superior photocatalytic Cr(VI) reduction capability, with the B1N3 composite showing the highest Cr(VI) reduction activity (99% within 100 min). This indicated that the introduction of N-$K_2Ti_4O_9$ into BUC-21 not only broadened the light absorption region to white light, but also promoted the transfer of photo-generated electrons and inhibited the recombination of electrons and holes. The acidity and alkalinity of the reaction solution was expected to strongly affect the Cr(VI) removal performances of the catalysts. As shown in Figs. 8c and 8f, the photocatalytic Cr(VI) reduction efficiencies did indeed vary significantly under different pH conditions. Under UV and white light irradiation, the photocatalytic performances of B1N0.5 and B1N3 decreased gradually with increasing pH. At lower pH conditions, the reaction proceeded in accordance with Eqs. 3, 4, and 5, in which the high availability of H^+ ions enhances the conversion of Cr(VI) to Cr(III). In contrast, at higher pH, the reaction proceeded via Eqs. 3, 5, and 6, in which the formed Cr(III) was declined to form precipitates that covered the active sites of B1N0.5 and B1N3 and inhibited further Cr(VI) reduction.

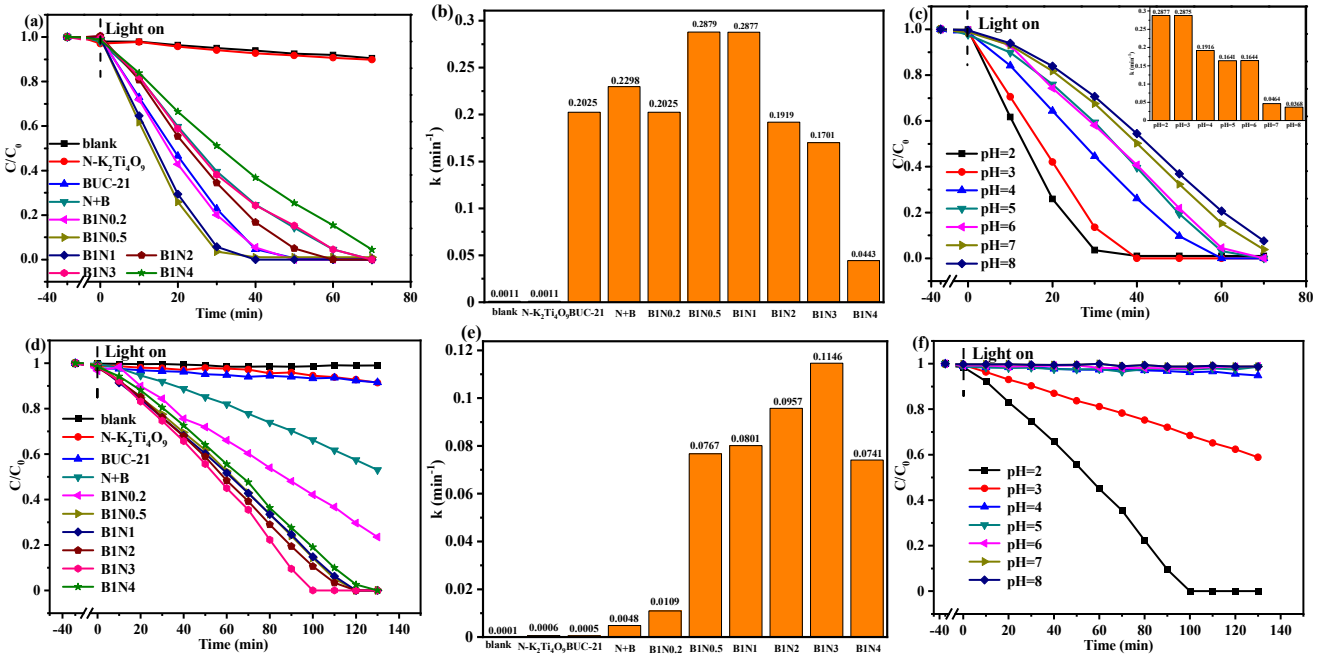

Fig. 8. (a) and (d) Photocatalytic Cr(VI) removal efficiencies of BUC-21, N-$K_2Ti_4O_9$, and the B1N*X* composites under UV and white light irradiation, respectively. (b) and (e) Reaction rate constants (*k*) of the different photocatalysts. (c) and (f) Effect of the initial pH on Cr(VI) removal under UV and white light irradiation, respectively. Conditions: photocatalyst = 0.175 g L^{-1}, Cr(VI) = 10 mg L^{-1}, 200 mL, pH = 2.0.

$$B1NX + h\nu \rightarrow B1NX\ (h^+ + e^-) \quad (3)$$

$$14H^+ + Cr_2O_7^{2-} + 6e^- \rightarrow 2Cr^{3+} + 7H_2O \quad (4)$$

$$2H_2O + 2h^+ \rightarrow H_2O_2 + 2H^+ \quad (5)$$

$$CrO_4^{2-} + 4H_4O + 3e^- \rightarrow Cr(OH)_3(s) + 5OH^- \quad (6)$$

The effective hole consumption could quickly capture photo-generated holes and enhance the utilization of electrons to

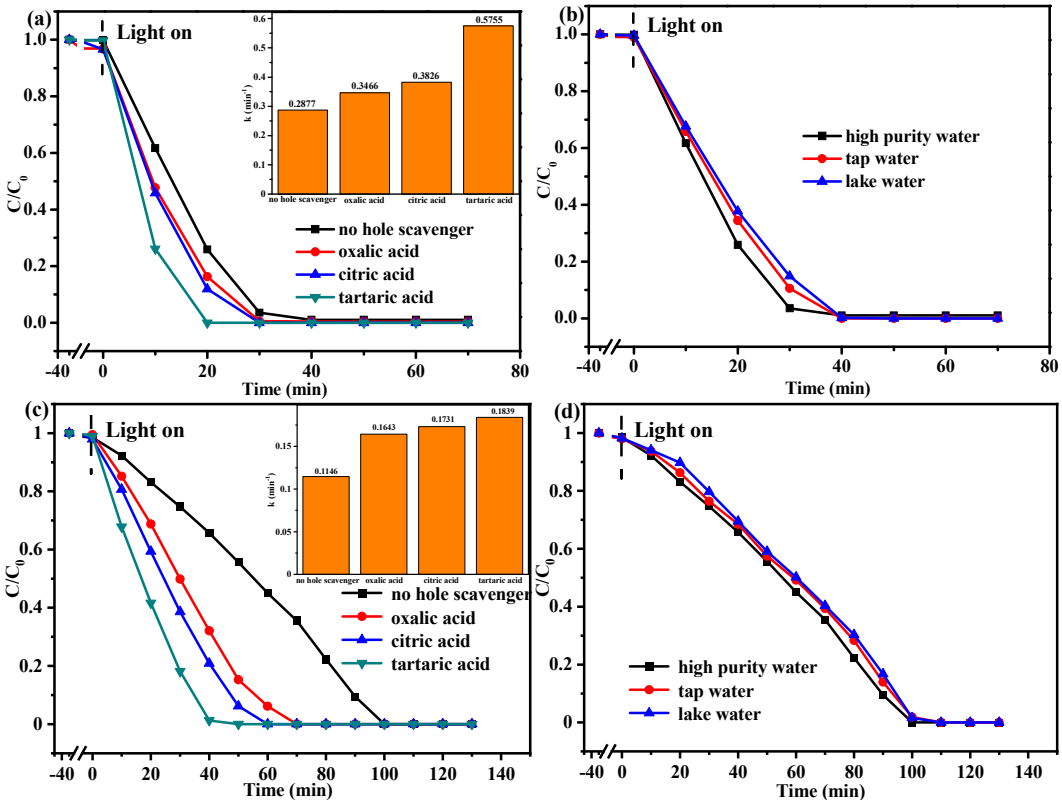

Fig. 9. (a) and (c) Photocatalytic Cr(VI) elimination over B1N0.5 and B1N3 in the presence of various hole scavengers under UV and white light irradiation, respectively. (b) and (d) Influence of water quality on Cr(VI) removal over B1N0.5 and B1N3. Conditions: Photocatalyst = 0.175 g L^{-1}, Cr(VI) = 10 mg L^{-1}, 200 mL, pH = 2.0.

achieve efficient removal of Cr(VI). Oxalic acid ($H_2C_2O_4$), citric acid ($C_6H_8O_7$), and tartaric acid ($C_4H_6O_6$) were selected to study the influence of different hole trappings on the reduction of Cr(VI) at pH 2.0. As shown in Figs. 9a and 9c, the addition of these small-molecule organic acids greatly improved the Cr(VI) reduction efficiencies of B1N0.5 and B1N3, with the enhancement following the order tartaric acid > citric acid > oxalic acid, which corresponded to the number of α-hydroxyl groups [53,62]. The depletion of the holes provided more photo-induced electrons to reduce Cr(VI), which led to the higher reduction efficiency and reaction rate.

In order to investigate the impact of co-existing ions, the wastewater stock solution with the same Cr(VI) concentration simulated from real lake water and tap water (collected from Daxing Campus, BUCEA) were used to explore the photocatalytic Cr(VI) removal performance of B1N0.5 and B1N3 under UV and white light irradiation, respectively. The parameters of the simulated wastewater are listed in Table S1. As shown in Fig. 9b, the presence of co-existing inorganic ions had a negligible effect, as demonstrated by the Cr(VI) removal efficiencies after 30 min, decreasing from 100% for the pure water solution to 90% and 86% for the tap water and lake water solutions, respectively. When the reaction time was prolonged to 40 min, Cr(VI) was completely reduced for all water quality conditions under UV irradiation, indicating that the co-existing ions had a negligible impact on the photocatalytic performance of B1N0.5. The same phenomenon could be observed under white light (Fig. 9d).

Photocatalysts for practical applications must also be recyclable and stable. B1N0.5 clearly maintained a 100% Cr removal rate after five experimental runs (Fig. 10a), and the PXRD patterns (Fig. 10b) and SEM and TEM images (Fig. S4) of the used B1N0.5 corresponded perfectly with those of the composites before reaction, implying that B1N0.5 possessed excellent stability, recyclability, and reusability. The recyclability and stability of B1N3 were also explored. As shown in Fig. 10c, the photocatalytic Cr(VI) reduction ability of B1N3 did not decline evidently after five recycles, indicating that B1N3 could be used repeatedly. Moreover, the PXRD pattern (Fig. 10d) of B1N3 before and after the photocatalytic processes demonstrated that the structure of B1N3 was not damaged even after the five cycles, which was further affirmed by TEM and SEM (Fig. S5).

3.3. *Photocatalytic mechanism*

Measurement of the AQEs of Cr(VI) reduction using light with specific wavelengths is important to evaluating the photocatalytic ability of a catalyst [63]. As illustrated in Fig. 11a and b, the AQEs of both B1N0.5 and B1N3 exhibited a positive correlation with the curves of their UV-vis DRS spectra, demonstrating that the Cr(VI) reduction was photo-induced. Furthermore, the AQE of B1N0.5 was much higher than that of B1N3 in the ultraviolet wavelength range. However, as the wavelength was gradually increased into the visible region, B1N3 achieved superiority; this fact helped to explain the different optimal catalyst compositions (B1N0.5 and B1N3) under UV irradiation and white light irradiation, respectively. Moreover, although the AQE of B1N3 decreased at 420 nm (Fig. 11b),

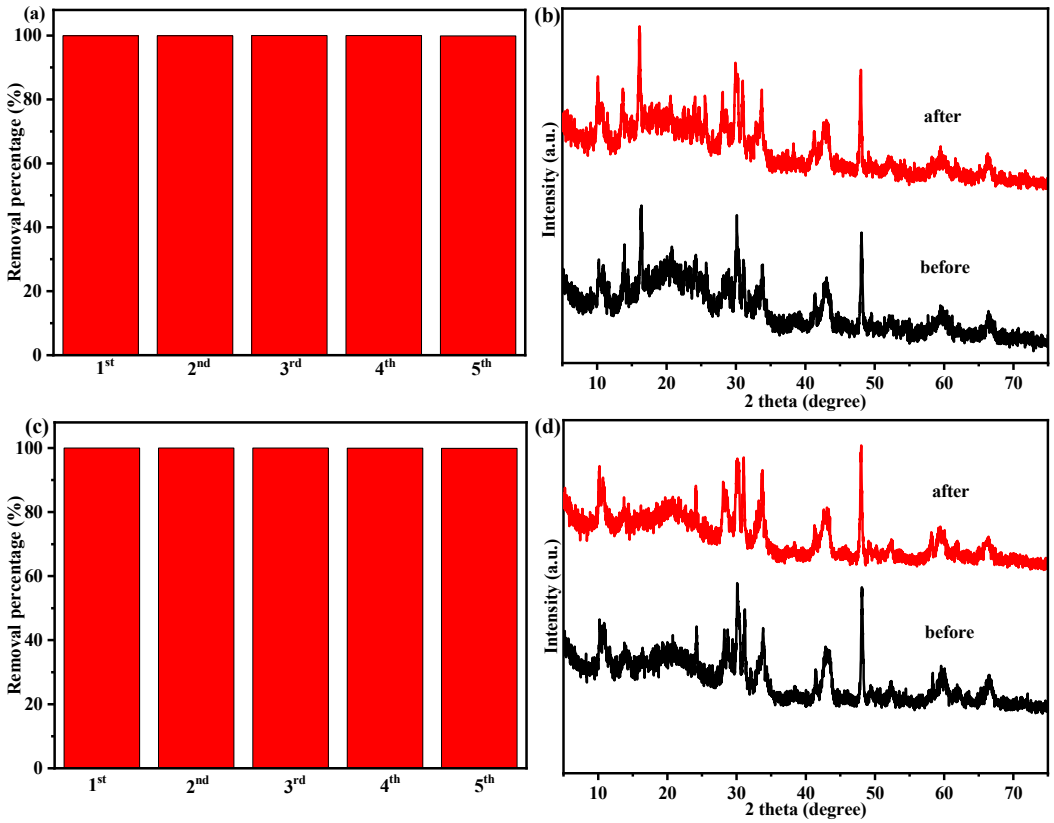

Fig. 10. (a) and (c) Reusability of B1N0.5 and B1N3 for the reduction of Cr(VI). (b) and (d) PXRD patterns of B1N0.5 and B1N3 before and after the five reactions.

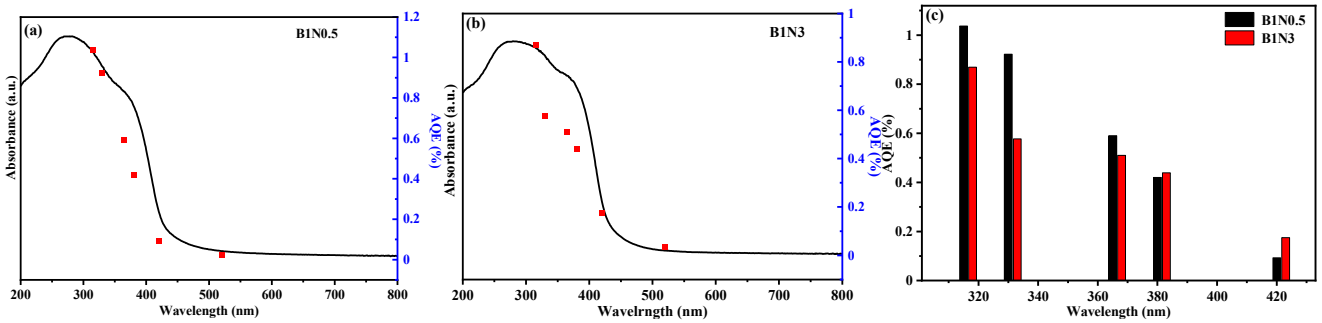

Fig. 11. AQE of Cr(VI) reduction over B1N0.5 (a) and B1N3 (b) under monochromatic light of various wavelengths and the corresponding column chart (c).

it still exhibited an efficiency of 0.2% at this frequency. The results proved that the removal of Cr(VI) over B1N3 upon white light irradiation could be attributed to both ultraviolet light and white light, resulting from the combination of BUC-21 and N-$K_2Ti_4O_9$.

Based on previous work, a lower PL signal implies lower recombination efficiency of photo-generated carriers [64]. As shown in Fig S6a, the PL intensities of B1N0.5 and B1N3 were lower than that of pure N-$K_2Ti_4O_9$, indicating that the BUC-21 and N-$K_2Ti_4O_9$ composites exhibited superior separation of the photo-generated electrons and holes than N-$K_2Ti_4O_9$ alone. Moreover, time-resolved photoluminescence analysis (Fig S6b) demonstrated that the average PL lifetimes of B1N0.5 and B1N3 were longer than that of pure BUC-21, which also proved the above point. Additionally, EIS plots for both B1N0.5 and B1N3 are depicted in Fig S6c and d. B1N0.5 and B1N3 demonstrated greater photocurrent responses than BUC-21 or N-$K_2Ti_4O_9$ alone under identical conditions, confirming that B1N0.5 and B1N3 accomplished superior charge separation efficiencies.

To investigate their photocatalytic mechanisms, ESR experiments using the DMPO technique were conducted to determine the active species formed over BUC-21, N-$K_2Ti_4O_9$, B1N0.5, and B1N3. As expected, no signals were detected in the dark. However, upon the illumination with UV and white light for 5 min or 10 min, $\bullet O_2^-$ signals were clearly observed over N-$K_2Ti_4O_9$, B1N0.5, and B1N3. Longer irradiation time led to stronger signal intensity, confirming that $\bullet O_2^-$ radicals were produced during the photocatalytic procedure [65]. Because BUC-21 could be excited by UV irradiation, an obvious DMPO $\bullet O_2^-$ signal was observed after 5 or 10 min under UV exposure; however, under white light irradiation, only a weak intensity signal was observed after 10 min. This was attributed to the fact that the white light covered only part of the UV light range.

Different types of photocatalysts produce different main active species because of the differences in their band structures

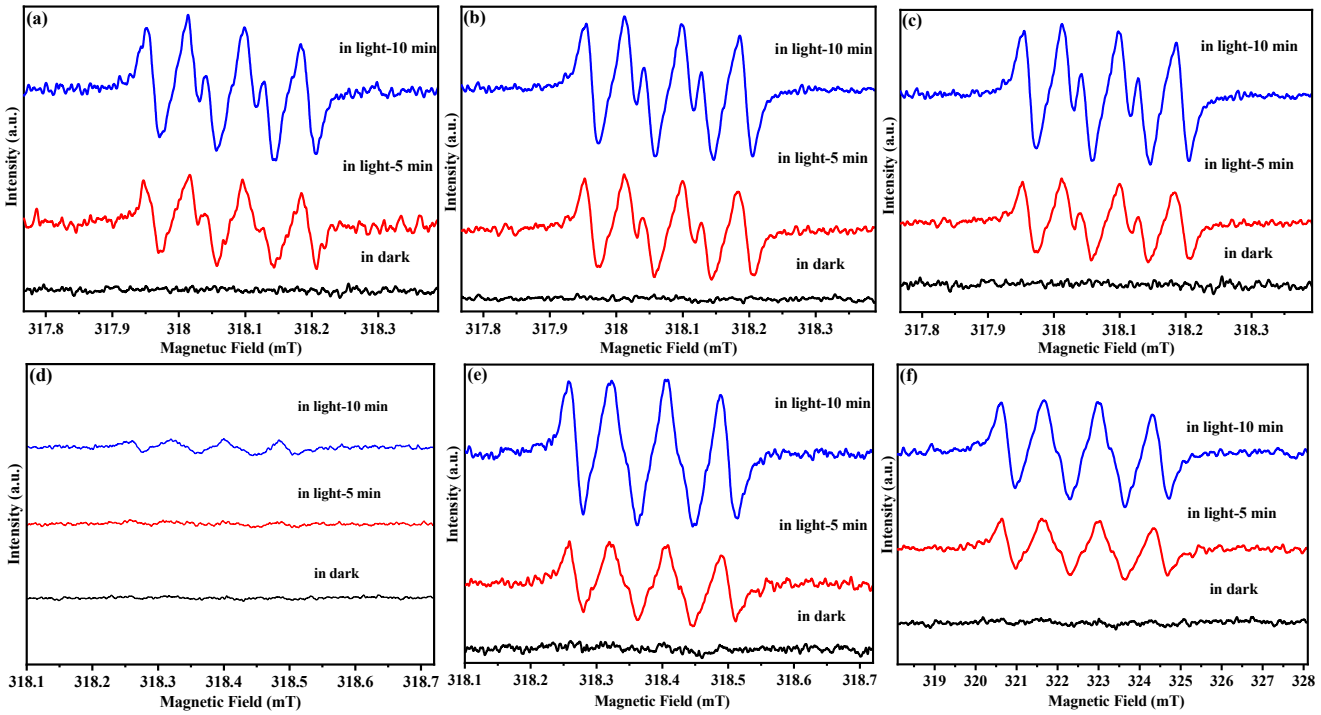

Fig. 12. ESR spectra of $\bullet O_2^-$ in aqueous dispersions over BUC-21 (a), N-$K_2Ti_4O_9$ (b), and B1N0.5 (c) under UV irradiation and over BUC-21 (d), N-$K_2Ti_4O_9$ (e), and B1N3 (f) under white light irradiation.

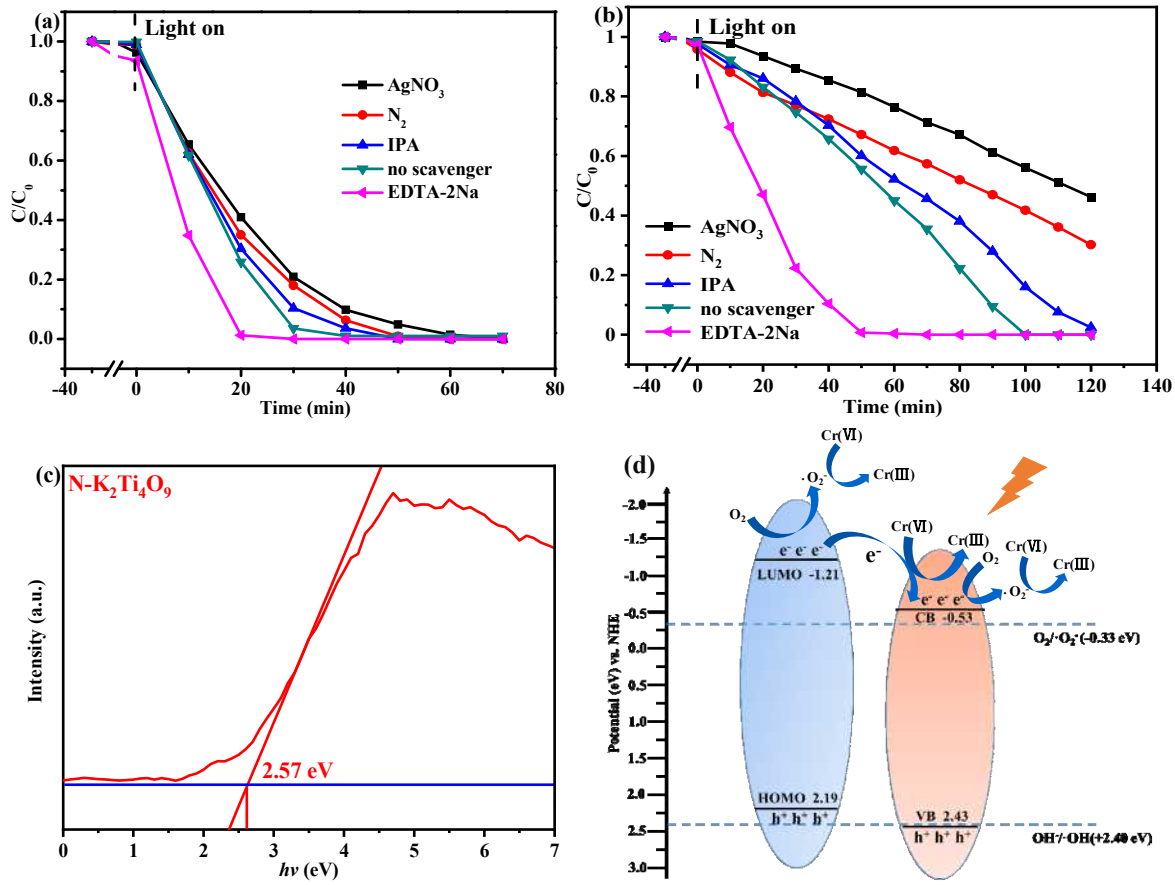

Fig. 13. (a) Effects of various capture agents on the reduction of Cr(VI) over (a) B1N0.5 and (b) B1N3. (c) Valence band XPS spectra of N-$K_2Ti_4O_9$. (d) Proposed mechanism of photocatalytic Cr(VI) elimination over BUC-21/N-$K_2Ti_4O_9$.

or phase compositions [66]. To explore the roles of various active substances in the photocatalytic Cr(VI) removal processes in this work, a set of capture experiments were conducted, in which e^-, •OH, and h^+ were captured using $AgNO_3$, IPA, and EDTA-2Na, respectively. Nitrogen gas was pumped into the reaction system to remove dissolved oxygen to prevent the formation of $•O_2^-$. As illustrated in Fig. 13a and b, e^- capture clearly inhibited the reduction of Cr(VI), revealing that Cr(VI) was mainly reduced to Cr(III) by continuous single electron transfer steps on N-$K_2Ti_4O_9$ (Eq. 7) [67]. Eqs. 8 and 9 demonstrate that $•O_2^-$ could also participate in Cr(VI) reduction [68]. This participation of $•O_2^-$ was confirmed by the fact that the Cr(VI) reduction performance also decreased after nitrogen gas was pumped into the reaction system. The $•O_2^-$ radicals could also generate •OH through a series of reactions (Eqs. 8, 10 and 11). When •OH was captured, it promoted the reaction in Eq. 11, thereby inhibiting the elimination of Cr(VI) [69]. The addition of EDTA-2Na promoted the Cr(VI) removal; this effect was attributed to the enhanced separation of the photo-induced electrons/holes and the adverse reaction illustrated in Eq. 13.

$$Cr(VI) \xrightarrow{e^-} Cr(V) \xrightarrow{e^-} Cr(IV) \xrightarrow{e^-} Cr(III) \quad (7)$$

$$O_2 + e^- \rightarrow \cdot O_2^- \quad (8)$$

$$\cdot O_2^- + Cr(VI) \rightarrow Cr(V) + O_2 \quad (9)$$

$$2\cdot O_2^- + 2H^+ \rightarrow H_2O_2 + O_2 \quad (10)$$

$$H_2O_2 + Cr(III) + H^+ \rightarrow Cr(VI) + H_2O + •OH \quad (11)$$

$$2H_2O + h^+ \rightarrow 2•OH + H^+ \quad (12)$$

$$Cr(V) + h^+/•OH \rightarrow Cr(VI) + OH^- \quad (13)$$

To further explore the reaction mechanism, the valence band (VB) of N-$K_2Ti_4O_9$ was determined using valence band XPS (VB-XPS). As shown in Fig. 13c, the valence band (VB) energy level was found to be 2.57 eV for N-$K_2Ti_4O_9$. Using Eqs. 14 and 15 [70], the VB and CB positions of N-$K_2Ti_4O_9$ were calculated to be 2.43 eV *vs* NHE and -0.53 eV *vs* NHE, respectively. The HOMO (2.19 eV) and LUMO (-1.21 eV) positions of BUC-21 matched well with our previous work [44]. A possible mechanism is shown in Fig. 13d. In the photocatalysis process, BUC-21 and N-$K_2Ti_4O_9$ are excited under UV or white light irradiation and produce photo-generated electrons and holes. Because of the difference between the E_{LUMO} of BUC-21 (−1.21 eV) and the E_{CB} of N-$K_2Ti_4O_9$ (−0.53 eV), the photo-generated electrons tend to move from the LUMO of BUC-21 to the CB of N-$K_2Ti_4O_9$, which facilitates the separation of the photo-generated electrons and holes of BUC-21 and promotes the reduction of Cr(VI) to Cr(III) via the electrons accumulated in the CB of N-$K_2Ti_4O_9$. Since the E_{LUMO} of BUC-21 and the E_{CB} of N-$K_2Ti_4O_9$ were more positive than the redox potential of $O_2/•O_2^-$ (-0.33 eV), the photo-generated electrons could react with dissolved oxygen (DO) to produce $•O_2^-$, which exerted a

positive effect on Cr(VI) reduction. However, the rate of $\bullet O_2^-$ production was slow for the LUMO of BUC-21 due to the fact that the white light covered only part of the ultraviolet light range capable of exciting BUC-21, which could also explain the slower Cr(VI) reduction rate over B1N3 under white light compared to that of B1N0.5 under UV light.

$$E_{NHE} = \Phi + E_{VL} - 4.44 \quad (14)$$

$$E_g = E_{VB} - E_{CB} \quad (15)$$

E_{NHE} is the potential of the normal hydrogen electrode; Φ is the electron work function of the analyzer (4.30 eV); E_{VL} is the potential of the vacuum level; E_g is the band-gap energy.

4. Conclusions

BUC-21/N-$K_2Ti_4O_9$ (B1N*X*) composites that could rapidly achieve Cr(VI) reduction under both UV and white light irradiation were easily prepared via ball milling. The obtained composites B1N0.5 and B1N3 displayed outstanding photocatalytic activity toward Cr(VI) reduction (100%) under UV and white light; the reduction was 1.4- and 14.3-fold quicker than that over pure BUC-21, respectively, as electron transfer between BUC-21 and N-$K_2Ti_4O_9$ decreased the chance of electron-hole pair recombination. Furthermore, experiments in the presence of co-existing ions and recycling experiments also demonstrated the good reusability and stability of B1N0.5 and B1N3, which could make them suitable for iterative processing. This study shows that N-$K_2Ti_4O_9$/MOF composite photocatalysts would be useful for the remediation of Cr-contaminated wastewater. BUC-21, with its two-dimensional crystal structure, should also provide further possibilities to accomplish the elimination of environmental pollutants with the aid of various nano-materials.

References

[1] C.-C. Wang, X.-D. Du, J. Li, X.-X. Guo, P. Wang, J. Zhang, *Appl. Catal. B*, **2016**, 193, 198–216.

[2] X. Yuan, H. Wang, J. Wang, G. Zeng, X. Chen, Z. Wu, L. Jiang, T. Xiong, J. Zhang, H. Wang, *Catal. Sci. Technol.*, **2018**, 8, 1545–1554.

[3] Q. Zeng, Y. Huang, H. Wang, L. Huang, L. Hu, H. Zhong, Z. He, *J. Hazard. Mater.*, **2020**, 383, 121199.

[4] Q. Sun, X. Hu, S. Zheng, J. Zhang, J. Sheng, *Environ. Pollut.*, **2019**, 245, 53–62.

[5] B. Wu, D. Peng, S. Hou, B. Tang, C. Wang, H. Xu, *Environ. Pollut.*, **2018**, 240, 717–724.

[6] Z. Ren, D. Kong, K. Wang, W. Zhang, *J. Mater. Chem. A*, **2014**, 2, 17952–17961.

[7] Y. Gao, W. Sun, W. Yang, Q. Li, *J. Mater. Sci. Technol.*, **2018**, 34, 961–968.

[8] J. Geng, F. Gu, J. Chang, *J. Hazard. Mater.*, **2019**, 375, 174–181.

[9] H. Wang, X. Yuan, Y. Wu, X. Chen, L. Leng, H. Wang, H. Li, G. Zeng, *Chem. Eng. J.*, **2015**, 262, 597–606.

[10] J. Xu, C. Liu, J. Niu, Y. Zhu, B. Zang, M. Xie, M. Chen, *J. Alloy. Compd.*, **2019**, 815, 152492.

[11] Q. Xu, R. Li, C. Wang, D. Yuan, *J Alloy Compd*, **2017**, 723, 441–447.

[12] M. Y. Akram, M. U. Hameed, N. Akhtar, S. Ali, I. Maitlo, X.-Q. Zhu, N. Jun, *J. Hazard. Mater.*, **2019**, 366, 723–731.

[13] C.-C. Wang, Y.-S. Ho, *Scientometrics*, **2016**, 109, 481–513.

[14] X.-D. Du, C.-C. Wang, J. Zhong, J.-G. Liu, Y.-X. Li, P. Wang, *J. Environ. Chem. Eng.*, **2017**, 5, 1866–1873.

[15] M. Li, Y. Liu, C. Shen, F. Li, C.-C. Wang, M. Huang, B. Yang, Z. Wang, J. Yang, W. Sand, *J. Hazard. Mater.*, **2019**, 10.1016/j.jhazmat.2019.121840.

[16] S. Chavan, J. G. Vitillo, D. Gianolio, O. Zavorotynska, B. Civalleri, S. r. Jakobsen, M. H. Nilsen, L. Valenzano, C. Lamberti, K. P. Lillerud, *Phys. Chem. Chem. Phys.*, **2012**, 14, 1614–1610.

[17] N. Chang, X.-P. Yan, *J. Chromatogr. A*, **2012**, 1257, 116–124.

[18] X.-F. Zhang, Y. Feng, Z. Wang, M. Jia, J. Yao, *J. Membr. Sci.*, **2018**, 568, 10–16.

[19] S.-W. Lv, J.-M. Liu, C.-Y. Li, N. Zhao, Z.-H. Wang, S. Wang, *Chem. Eng. J.*, **2019**, 375, 122111.

[20] X. Qiao, Y. Han, D. Tian, Z. Yang, J. Li, S. Zhao, *Sens. Actuators B*, **2019**, 286, 1–8.

[21] H. Wang, X. Yuan, G. Zeng, Y. Wu, Y. Liu, Q. Jiang, S. Gu, *Adv. Colloid Interface Sci.*, **2015**, 221, 41–59.

[22] L. Shen, W. Wu, R. Liang, R. Lin, L. Wu, *Nanoscale*, **2013**, 5, 9374–9382.

[23] P. Li, M. Guo, Q. Wang, Z. Li, C. Wang, N. Chen, C.-C. Wang, C. Wan, S. Chen, *Appl. Catal. B*, **2019**, 259, 118107.

[24] J. Qiu, X. Zhang, Y. Feng, X. Zhang, H. Wang, J. Yao, *Appl. Catal. B*, **2018**, 231, 317–342.

Graphical Abstract

Chin. J. Catal., 2021, 42: 259–270 doi: 10.1016/S1872-2067(20)63629-4

Photocatalytic Cr(VI) elimination over BUC-21/N-$K_2Ti_4O_9$ composites: Big differences in performance resulting from small differences in composition

Xun Wang, Yu-Xuan Li, Xiao-Hong Yi, Chen Zhao, Peng Wang, Jiguang Deng *, Chong-Chen Wang *
Beijing University of Civil Engineering and Architecture;
Beijing University of Technology

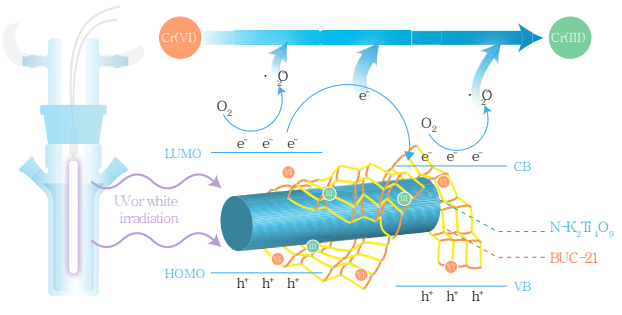

BUC-21/N-$K_2Ti_4O_9$ composites show high photocatalytic activity under UV and white light, which can be used to reduce Cr(VI) to Cr(III) effectively.

[25] Z. Wang, L. Song, Y. Wang, X.-F. Zhang, D. Hao, Y. Feng, J. Yao, *Chem. Eng. J.*, **2019**, 371, 138–144.
[26] X. Wang, W. Liu, H. Fu, X.-H. Yi, P. Wang, C. Zhao, C.-C. Wang, W. Zheng, *Environ. Pollut.*, **2019**, 249, 502–511.
[27] Y.-C. Zhou, P. Wang, H. Fu, C. Zhao, C.-C. Wang, *Chin. Chem. Lett.*, **2020**, 10.1016/j.cclet.2020.02.048.
[28] Q. Mu, W. Zhu, X. Li, C. Zhang, Y. Su, Y. Lian, P. Qi, Z. Deng, D. Zhang, S. Wang, X. Zhu, Y. Peng, *Appl. Catal. B*, **2020**, 262, 118144.
[29] W. Chen, B. Han, C. Tian, X. Liu, S. Liang, H. Deng, Z. Lin, *Appl. Catal. B*, **2019**, 244, 996–1003.
[30] X. Zhang, J. Wang, X.-X. Dong, Y.-K. Lv, *Chemosphere*, **2020**, 242, 125144.
[31] Y. Li, Y. Fang, Z. Cao, N. Li, D. Chen, Q. Xu, J. Lu, *Appl. Catal. B*, **2019**, 250, 150–162.
[32] L. Luo, Y. Wang, S. Huo, P. Lv, J. Fang, Y. Yang, B. Fei, *Int. J. Hydrogen Energy*, **2019**, 44, 30965–30973.
[33] Z. Wang, Z. Jin, G. Wang, B. Ma, *Int. J. Hydrogen Energy*, **2018**, 43, 13039–13050.
[34] C.-C. Wang, X.-H. Yi, P. Wang, *Appl. Catal. B*, **2019**, 247, 24–48.
[35] H. Wang, X. Yuan, Y. Wu, G. Zeng, X. Chen, L. Leng, H. Li, *Appl. Catal. B*, **2015**, 174–175, 445–454.
[36] Y.-C. Zhou, X.-Y. Xu, P. Wang, H. Fu, C. Zhao, C.-C. Wang, *Chin. J. Catal.*, **2019**, 40, 1912–1923.
[37] C.-C. Wang, X. Wang, W. Liu, *Chem. Eng. J.*, **2020**, 10.1016/j.cej.2019.123601.
[38] C. Zhao, Z. Wang, X. Li, X.-H. Yi, H. Chu, X. Chen, C.-C. Wang, *Chem. Eng. J.*, **2020**, 10.1016/j.cej.2019.123431
[39] D.-D. Chen, X.-H. Yi, C. Zhao, H. Fu, P. Wang, C.-C. Wang, *Chemosphere*, **2020**, 245, 125659.
[40] S. Zhang, Y. Wang, Z. Cao, J. Xu, J. Hu, Y. Huang, C. Cui, H. Liu, H. Wang, *Chem. Eng. J.*, **2020**, 381, 122771.
[41] Q. Li, S. Gong, H. Zhang, F. Huang, L. Zhang, S. Li, *Chem. Eng. J.*, **2019**, 371, 26–33.
[42] S. Zheng, P. Yang, F. Zhang, D.-L. Chen, W. Zhu, *Chem. Eng. J.*, **2017**, 328, 977–987.
[43] F.-X. Wang, X.-H. Yi, C.-C. Wang, J. G. Deng, *Chin. J. Catal.*, **2017**, 38, 2141–2149.
[44] X.-H. Yi, F.-X. Wang, X.-D. Du, P. Wang, C.-C. Wang, *Appl. Organomet. Chem.*, **2019**, 33, e4621.
[45] W. Cui, S. Ma, L. Liu, J. Hu, Y. Liang, *J. Mol. Catal. A*, **2012**, 359, 35–41.
[46] S. Li, X. Wang, Q. He, Q. Chen, Y. Xu, H. Yang, M. Lü, F. Wei, X. Liu, *Chin. J. Catal.*, **2016**, 37, 367–377.
[47] F. Wang, Y. T. Zhang, Y. Xu, X. Wang, S. Li, H. Yang, X. Liu, F. Wei, *J. Environ. Chem. Eng.*, **2016**, 4, 3364–3373.
[48] Q. Chen, Q. He, M. Lv, X. Liu, J. Wang, J. Lv, *Appl. Surf. Sci.*, **2014**, 311, 230–238.
[49] M. R. Allen, A. Thibert, E. M. Sabio, N. D. Browning, D. S. Larsen, F. E. Osterloh, *Chem. Mater.*, **2014**, 22, 1220–1228.
[50] D. Mitoraj, H. Kisch, *Angew. Chem. Int. Ed.*, **2008**, 47, 9975–9978.
[51] Y.-X. Li, H. Fu, P. Wang, C. Zhao, W. Liu, C.-C. Wang, *Environ. Pollut.*, **2020**, 256, 113417.
[52] S. Ouyang, J. Ye, *J. Am. Chem. Soc.*, **2011**, 133, 7757–7763.
[53] X. H. Yi, S.-Q. Ma, X. D. Du, C. Zhao, H. Fu, P. Wang, C. C. Wang, *Chem. Eng. J.*, **2019**, 375, 121944.
[54] W. Fang, T. Z. Yong, Y. Xu, W. Xing, S. Li, H. Yang, X. Liu, F. Wei, *J. Environ. Chem. Eng.*, **2016**, 4, 3364–3373.
[55] Y. Xu, C. Qi, H. Yang, M. Lv, Q. He, X. Liu, F. Wei, *Mater. Sci. Semicon. Proc.*, **2015**, 36, 115–123.
[56] Q. Chen, Q. He, M. Lv, X. Liu, W. Jin, J. Lv, *Appl. Surf. Sci.*, **2014**, 311, 230–238.
[57] S. Li, X. Wang, Q. Chen, Q. He, M. Lv, X. Liu, J. Lv, F. Wei, *RSC Adv.*, **2015**, 5, 53198–53206.
[58] M. Sun, Y. Fang, S. Sun, Y. Wang, *RSC Adv.*, **2016**, 6, 12272–12279.
[59] X. Liu, Z. Xing, Y. Zhang, Z. Li, X. Wu, S. Tan, X. Yu, Q. Zhu, W. Zhou, *Appl. Catal. B*, **2017**, 201, 119–127.
[60] Z. Jiang, W. Wei, D. Mao, C. Chen, Y. Shi, X. Lv, J. Xie, *Nanoscale*, **2015**, 7, 784–797.
[61] X.-D. Du, X.-H. Yi, P. Wang, J. G. Deng, C.-C. Wang, *Chin. J. Catal.*, **2019**, 40, 70–79.
[62] C. E. Barrera-Díaz, V. Lugo-Lugo, B. Bilyeu, *J. Hazard. Mater.*, **2012**, 223–224, 1–12.
[63] C. J. Murphy, J. M. Buriak, *Chem. Mater.*, **2015**, 27, 4911–4913.
[64] Q. Liu, C. Zeng, L. Ai, Z. Hao, J. Jiang, *Appl. Catal. B*, **2018**, 224, 38–45.
[65] X.-D. Du, X.-H. Yi, P. Wang, W. Zheng, J. Deng, C.-C. Wang, *Chem. Eng. J.*, **2019**, 356, 393–399.
[66] S. Lin, L. Liu, J. Hu, Y. Liang, W. Cui, *J. Mol. Struct.*, **2015**, 1081, 260–267.
[67] J.-C. Wang, J. Ren, H.-C. Yao, L. Zhang, J.-S. Wang, S.-Q. Zang, L.-F. Han, Z.-J. Li, *J. Hazard. Mater.*, **2016**, 311, 11–19.
[68] G. Dong, L. Zhang, *J. Phys. Chem. C*, **2013**, 117, 4062–4068.
[69] X. Hu, H. Ji, F. Chang, Y. Luo, *Catal. Today*, **2014**, 224, 34–40.
[70] L. Wang, G. Zhou, Y. Tian, L. Yan, M. Deng, B. Yang, Z. Kang, H. Sun, *Appl. Catal. B*, **2019**, 244, 262–271.

BUC-21/N-$K_2Ti_4O_9$复合材料光催化去除Cr(VI): 组成上的细微差异导致性能上的巨大差异

王 恂[a], 李玉璇[a], 衣晓虹[a], 赵 晨[a], 王 鹏[a], 邓积光[b,*], 王崇臣[a,#]
[a]北京建筑大学建筑结构与环境修复功能材料北京重点实验室, 北京100044
[b]北京工业大学环境与能源工程学院化学与化工系, 北京100022

摘要: 近年来, 金属-有机骨架(MOFs)作为一种多相光催化剂因其合成方法多样、活性位点可调等优点被越来越多地应用于光催化还原Cr(VI)、还原CO_2和降解有机污染物等领域. 但多数MOFs被其电导率低、电子与空穴的快速复合以及仅在紫外光下激发下才能表现出光催化活性等缺点限制了其进一步应用. 为此, 与g-C_3N_4、Ag_2CO_3、TiO_2、$Bi_{24}O_{31}Br_{10}$等半导体、电活性聚合物(PANI)、导体(RGO)、贵金属纳米颗粒(Ag, Pd)等构建复合物是增强MOFs光催化性能的一个有效策略.

本文采用简单的机械球磨法, 以BUC-21和N-$K_2Ti_4O_9$为前驱体快速制备了一系列BUC-21/N-$K_2Ti_4O_9$复合材料(记为B1N*X*, 其中*X* = 0.2, 0.5, 1, 2, 3和4, 代表N-$K_2Ti_4O_9$在复合物中的比例). 采用粉末X射线衍射(PXRD)、傅里叶变换红外光谱(FTIR)、扫描电镜(SEM)、透射电镜(TEM)、高倍透射电镜(HRTEM)、紫外-可见漫反射(UV-Vis DRS)和X射线光电子能谱

(XPS)等技术对UAC-X复合物的形貌和结构进行了表征. 研究了B1N*X*在紫外光和白光照射下光催化还原六价铬(Cr(VI))的性能. 探究了不同pH (pH = 2–8)、不同小分子有机酸(柠檬酸、酒石酸和草酸)及共存离子(自来水和湖水中的离子)对光催化还原Cr(VI)的影响. 结果表明, PXRD谱图显示B1N*X*的衍射峰位置分别与BUC-21和N-$K_2Ti_4O_9$峰位置完全吻合. SEM、TEM、EDS和HRTEM图片证明在B1N*X*复合物中BUC-21附着在N-$K_2Ti_4O_9$表面. 在紫外光照射下40 min后, B1N0.5的光催化活性最高, 还原效率达到100.0%, 且还原速率是BUC-21的1.42倍. 而在白光照射下, 随着N-$K_2Ti_4O_9$含量的增加, 复合物的光催化活性先增后减. 最佳比例B1N3可在100 min时还原99%的Cr(VI), 远远优于对Cr(VI)几乎无还原能力的BUC-21和N-$K_2Ti_4O_9$. 这是因为N-$K_2Ti_4O_9$含量的增加不仅有利于电荷的转移, 也有利于白光的利用. 在紫外光和白光照射下, 随着溶液pH值从2提高到8, 还原效率逐渐降低. 这是因为在酸性条件下H^+浓度高有利于Cr(VI)还原为Cr(III), 而当pH>6时, Cr^{3+}与OH^-形成$Cr(OH)_3$沉淀附着在催化剂表面, 影响对光的吸收, 降低了光催化效率. 当反应体系中加入草酸、柠檬酸和酒石酸等小分子有机酸时, 光催化速率得到显著提高, 这是由于小分子链烃有机物容易捕捉光生空穴. 共存离子实验表明, 虽然湖水和自来水中的共存离子对B1N0.5和B1N3的还原性能稍有抑制, 但当反应时间延长时, 这种影响可忽略不计. 表观量子效率实验证明B1N*X*还原Cr(VI)是光诱导过程. 光致发光分析、时间分辨光致发光分析、电化学分析、电子自旋共振(ESR)和活性物质捕获实验显示, B1N0.5和B1N3中BUC-21最低未占轨道(LUMO)上的光生电子转移至N-$K_2Ti_4O_9$导带, 提高了光生电子和空穴的分离效率, 最终增强了光催化还原Cr(VI)的活性. N-$K_2Ti_4O_9$的引入也使得BUC-21的光吸收区域拓展至白光, 实现了其实际应用的潜力. 同时, B1N0.5在紫外光照射下和B1N3在白光照射下经过5次光催化循环实验后其还原Cr(VI)效率仍然可达99%, 且PXRD谱图、SEM和TEM图像未见明显变化, 表明其具有稳定性和重复利用性. 综上, BUC-21/N-$K_2Ti_4O_9$是一种具有应用前景的高效复合型光催化剂.

关键词: BUC-21; N-$K_2Ti_4O_9$; 光催化; 六价铬; 紫外光和白光

收稿日期: 2020-03-23. 接受日期: 2020-05-05. 出版日期: 2021-02-05.

*通讯联系人. 电话/传真: (010)61209186; 电子信箱: jgdeng@bjut.edu.cn

#通讯联系人. 电子信箱: wangchongchen@bucea.edu.cn, chongchenwang@126.com

基金来源: 国家自然科学基金(51878023); 北京自然科学基金(8202016); 北京市属高等学校长城学者培养计划(CIT&TCD20180323); 北京市百千万人才工程(2019A22); 北京建筑大学研究生创新项目(PG2019038).

本文的电子版全文由Elsevier出版社在ScienceDirect上出版(http://www.sciencedirect.com/science/journal/18722067).